Journal of Applied Fluid Mechanics, Vol. 18, No. 1, pp. 16-31, 2025.
Available online at www.jafmonline.net, ISSN 1735-3572, EISSN 1735-3645.
https://doi.org/10.47176/jafm.18.1.2749

Experimental Investigation to Utilize Low-cost Sensors of Early Cavitation Prediction in Axial Pump Based on Acoustic and Vibration Approaches

A. R. Al-Obaidi[1] and J. Alhamid[2]

[1] *Department of Mechanical Engineering, College of Engineering, Mustansiriyah University, Baghdad, Iraq*
[2] *Washington State University, School of Mechanical and Materials Engineering, WSU Tri-Cities, USA*

Corresponding author E-mail: ahmedram@uomustansiriyah.edu.iq

ABSTRACT

Cavitation, defined by the formation and collapse of vapor bubbles in a liquid, presents a significant challenge to the reliable operation of axial pumps. Timely detection of cavitation is essential for preventing damage and optimizing pump performance. This research aims to evaluate detection techniques for cavitation in axial pumps through the analysis of vibration and acoustic signals. We utilized cost-effective sensors and data acquisition systems, including embedded accelerometer sensors and smartphone-based microphones, to capture these signals. Our study involves a detailed analysis of vibration and acoustic data collected under various operating conditions, with a particular focus on the pump's optimal efficiency point. By employing three directional axes for vibration data acquisition, we achieved a comprehensive examination of the cavitation phenomenon. Signal processing techniques, such as feature extraction in the frequency domain, were used to identify distinct operating conditions as cavitation developed. Additionally, convolutional features were applied to assess the classification accuracy when datasets were converted into spectrograms. This research includes a thorough comparison of classification algorithms and different directional axes to provide insights into the effectiveness of the detection methods. The findings demonstrate the feasibility of detecting cavitation in real operating conditions using vibration signals, while highlighting challenges associated with using low-cost commercial acoustic data for cavitation detection. This introduction sets the stage for an in-depth exploration of the methodology, results, and implications of our study on early cavitation detection in axial irrigation pumps. The analysis of acoustic and vibration signals yielded similar results in detecting cavitation. Key indicators, such as peak-to-peak, RMS, and variation values, were effective metrics for cavitation detection. Frequency-based analysis in both the broadband range (2 kHz – 10 kHz) and the low-frequency range (0 – 1 kHz) revealed clear trends related to cavitation presence. Time-domain analysis of vibration signals proved effective for detecting and diagnosing cavitation in axial pumps. Using mean and peak values for vibration and acoustic amplitude analysis in the frequency domain provided additional insights for predicting cavitation.

Article History

Received March 31, 2024
Revised August 12, 2024
Accepted August 13, 2024
Available online November 6, 2024

Keywords:

Axial flow pump
Cavitation monitoring
Vibration analysis
Acoustic signals
Cavitation detection

1. INTRODUCTION

To mitigate and manage cavitation in axial water pumps used for irrigation, prompt detection of this phenomenon is imperative. Various techniques for monitoring pump operational status exist, which can be implemented either during operation or through examination of internal components. However, conventional reactive maintenance

Nomenclature

f	frequency	Pv	vapour pressure
Hs	static suction head	p	static pressure
H	head of pump	Qed	design flow rate
NPSHr	Net Positive Suction Head Required	t	time
Q	mass flow rate	ρ	fluid density
T	pump shaft torque	BEP	Best Efficiency Point
Pint	total pressure at inlet	BPF	Blade Passing Frequency
Pout	total pressure at outlet	N	rotational pump speed
Patm	atmospheric pressure		

strategies and intrusive methodologies present significant limitations compared to non-intrusive alternatives. The shift towards proactive maintenance strategies necessitates a comprehensive investigation, given the prerequisites for process digitization, scheduling, and a structured maintenance framework (Shagluf et al., 2018). Non-invasive approaches, including vibration analysis, acoustic emissions, and sensor detection utilizing motor signal irregularities, are increasingly popular due to the capacity to reduce system downtime and related costs (Harihara & Parlos, 2008). Over recent decades, numerous non-invasive maintenance techniques have been thoroughly investigated, with varying degrees of detail and scope. Adeodu et al. (2020) notably pioneered the development of a digital twin for an axial pump, enabling precise forecasts of its operational status using predefined parameters. Mousmoulis et al. (2019) provided valuable insights into the relationship between impeller geometry and cavitation severity through macroscopic identification of cavitation formation. Fluid dynamics simulations have proven effective in analyzing vibration and sound data for diverse compressor variants, including pumps and fans (Xu et al., 2020). Additionally, convolutional neural networks (CNN) and artificial neural networks (ANN) have advanced significantly in image and signal analysis, respectively, showing remarkable success in identifying operational conditions across various pump configurations (Hallaji et al., 2022). The cavitation model provides a mathematical framework for understanding the transition from liquid to vapor within cavitation flows. Following the homogenization flow density definition method, this model is classified into two main types: the transport equation model and the state equation model (Pouffary et al., 2008). While the state equation model simulates cavitation conditions by establishing a functional correlation between pressure and density, its practical applicability is limited by the lack of a clear physical interpretation of the assumed density and pressure relationship. Consequently, the transport equation model has become the preferred choice for numerical simulation of cavitation flow (Kunz et al., 2000; Schnerr & Sauer, 2001; Coutier et al., 2005). Katz (1984) discovered that axial shear vortex formations influence cavitation progression within the separation zone. Laberteaux et al. (1998) used photography to detect eddy cavitation flow patterns in enclosed cavitation regions, revealing unsteady, turbulent flow characterized by complex exchanges of mass, momentum, and energy between bubbles and liquid. Predicting and simulating cavitation flow vortexes significantly impacts simulation methods. Modal analysis anticipates the resonance conditions of axial pumps by extracting mode shapes, natural frequencies, and critical speeds, representing an effective approach for analyzing vibration characteristics (Oza & Shah, 2020). Sendilvelan et al. (2017) conducted modal analysis on axial pump impellers of varying thicknesses, identifying natural frequencies and mode shapes. Zhang et al. (2022) investigated the natural vibration and critical speeds of a multistage axial pump rotor under different support stiffness conditions, highlighting significant impacts on the first and second critical speeds. Tian & Hu (2018) discovered that both support stiffness and fluid dynamics substantially influence the critical speed of multistage axial pump rotors. This investigation explores the utility of both acoustic and vibration data sourced from an axial pump using an accelerometer and a microphone device. The objective is to determine which signal type is more effective for cavitation detection. Acoustic data capture sound-related phenomena using any type of microphone positioned near the pump, while mechanical oscillations are understood via vibration data using accelerometers affixed to the vibrating source. Detecting cavitation in axial pumps and determining its occurrence timeframe is essential for implementing proactive maintenance strategies and refining the design of mechanical elements, such as impeller blades. This study examines how design parameters affect both cavitation formation and overall pump efficiency. The primary goal is to identify a reliable algorithm for early cavitation detection using minimally processed vibration data and signals. Experiments were conducted to assess the viability of acoustic and vibration techniques for cavitation diagnosis and detection, focusing on simulating real irrigation systems and finding affordable devices capable of concurrently capturing both types of data. Combining these data with robust algorithms demonstrates potential for real-time early detection, opening possibilities for preventive maintenance and proactive control measures. The systematic analysis of vibration and acoustic spectra under various operational conditions offers valuable insights into these methods' potential for cavitation detection and diagnosis. The investigation analyzed signals obtained under various operating conditions, comparing them to the manufacturer's operating curve and mathematical calculations for optimal pump efficiency. Data classification methods applied to vibration signals demonstrated a high success rate in

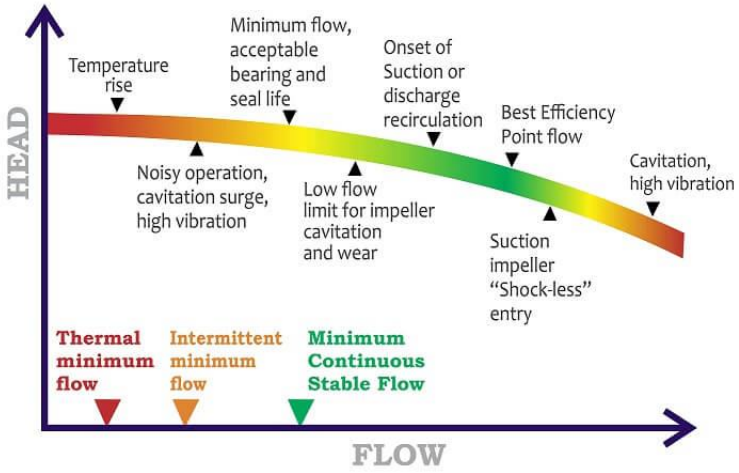

Fig. 1 Pump operation at conditions of cavitation without cavitation

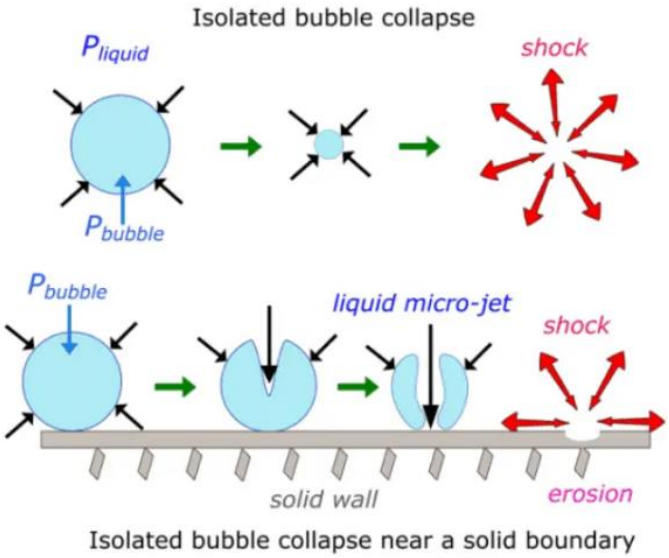

Fig. 2 Cavitation process

discerning different operating conditions, particularly concerning evolving cavitation phenomena. This analysis contributes valuable insights into the robustness and reliability of classification techniques when applied to vibration data for cavitation detection and characterization. Previous research predominantly employed laboratory setups with advanced acquisition systems incorporating industrial-grade sensors and sophisticated cameras. Maintaining operational safety and reliability requires a safety margin, typically around 10% towards the left of the duty point, to prevent issues like low bearing life, mechanical seal failure, and excessive vibration when operating on the left side of the performance curve. Conversely, operating too far to the right risks cavitation, which can rapidly damage the pump casing and impeller.

1.1 Pumps Work under Cavitation Conditions

Cavitation is the primary cause of the pronounced sound and vibration in pumps. It occurs when vapor bubbles form inside the pump and subsequently collapse. This collapsing action generates powerful pressure jets and shockwaves within the pump system, leading to elevated noise levels and increased vibrations, as illustrated in Fig. 2. These phenomena highlight the detrimental impact of cavitation on the operational stability and efficiency of the pump.

Cavitation erosion occurs when the implosions of cavities are forceful and happen near solid materials. This erosion is characterized by the distinct marks it leaves on the surfaces of flow path components. Despite extensive experimental research, the mechanism underlying cavitation erosion remains partially understood. Two potential mechanisms are considered: prolonged pump operation

under cavitation conditions can result in substantial damage, particularly to the impeller. Continued exposure to cavitation can lead to the development of pits on various components, such as the discharge edge of the blade, blade suction edge, casing, and blade of the impeller shroud. In severe cases, it may lead to the formation of holes in the impeller and significant damage to the vanes, rendering the impeller completely ineffective. These detrimental effects underscore the importance of addressing cavitation promptly to prevent extensive damage and maintain the pump's operational integrity.

As discussed, various indicators signal the onset and progression of cavitation within a pump. The methodologies employed for detecting and diagnosing cavitation rely on these observable signs. Substantial research has been dedicated to the detection of cavitation in water pumps and turbines, aiming to enhance understanding and develop effective diagnostic techniques to address this phenomenon.

2. EXPERIMENTAL CONFIGURATION AND ANALYSIS OF EXPERIMENTAL UNCERTAINTY

The experimental setup employed a comprehensive water pumping station configuration. Valves were strategically integrated into both the discharge and suction lines to simulate a wide range of operational scenarios. A sensor was placed in the discharge line to measure water flow, and additional sensors were used to consistently track pressure levels in both the discharge and suction lines. Figure 3 illustrates the experimental setup with a simplified piping and instrumentation diagram.

During this phase of the research, laboratory experiments were conducted on an axial pump using various sensors. The collected experimental data included pressure, acoustic signals, and vibration. To ensure the accuracy of the acoustic signals from the pump and mitigate the influence of ambient and motor noise, sound insulation covers were installed in the laboratory and around the motor. The effectiveness of these insulation covers in minimizing motor noise interference is evident from the presented tables. Together, these components form a crucial part of the experimental setup.

2.1. Experimental Uncertainty

The sketch of the experimental pump device is displayed in Fig. 1. The pipe segment in front of the electromagnetic flow meter was sufficiently long and straight to ensure both the accuracy of the test and a smooth flow into the apparatus. The flow meter was checked prior to installation and used for measuring flow. An electric motor and shaft were installed, and a differential pressure transmitter with a speed torque sensor measured the head of the pumping system by recording the pump shaft's speed and input torque. Systematic square root error and random error are involved in the head and efficiency synthesis error (Tian & Hu 2018).

$$E\eta = \pm\sqrt{E_{\eta,s}^2 + E_{\eta,R}^2} \quad (1)$$

The sum of the square roots of the separate system defects determines the overall error in the system of pump performance test on the test work (Tian et al., 2018):

$$E\eta, s = \pm\sqrt{E_{Q,s}^2 + E_{H,s}^2 + E_{n,s}^2 + E_{M,s}^2} \quad (2)$$

where $E_{Q,S}$ stands for electromagnetic flowmeter systematic error, $E_{H,S}$ for differential pressure transmitter systematic error, $E_{n,S}$ for sensor of torque systematic error, and $E_{M,S}$ for torque meter systematic error. Table 1 displays the testing equipment that is required to determine these systematic error parameters (Tian & Hu 2018).

Using test data from this model of pumping system, total random error was computed using the probability statistics method. $E\eta, s$ was approximately 0.21% unknown overall (Tian & Hu 2018).

The pump was tested multiple times at 3000 r/min using the same work test procedure and operating parameters to confirm the dependability of the test bench. Figure 4 displays the test findings. The pump, tested three times, shows nearly identical patterns in its flow-head curves as flow increases. The consistency of data gathered under comparable working conditions suggests that the test results are reliable.

The experiment utilized a data acquisition platform equipped with a Global Sensor Technology (GST) device attached to the pump casing with a metal plate. An Integrated Electronics Piezo-Electric (IEPE) accelerometer was employed to gather acceleration data, with the frequency sampling set to the highest range of 40 kHz. To gather acoustic data, an integrated microphone, initially intended for recording ambient sounds in videos and stereo acoustic recordings, was repurposed for this experiment. The microphone had a frequency response range, and a sampling frequency of 20 to 20 kHz was chosen. The

Table 1 Primary apparatus within the experimental work

Parameter	Device	Error
Head	Inlet pressure transducer Outlet pressure transducer	± 0.12 % ± 0.12 %
Flow	Flow meter	± 0.15 %
Speed and torque	Sensor of torque speed	± 0.17 %
Vibration Sensor	Accelerometer Sensor	± 0.20 %
Acoustic Sensor	microphone sensor	± 0.21 %

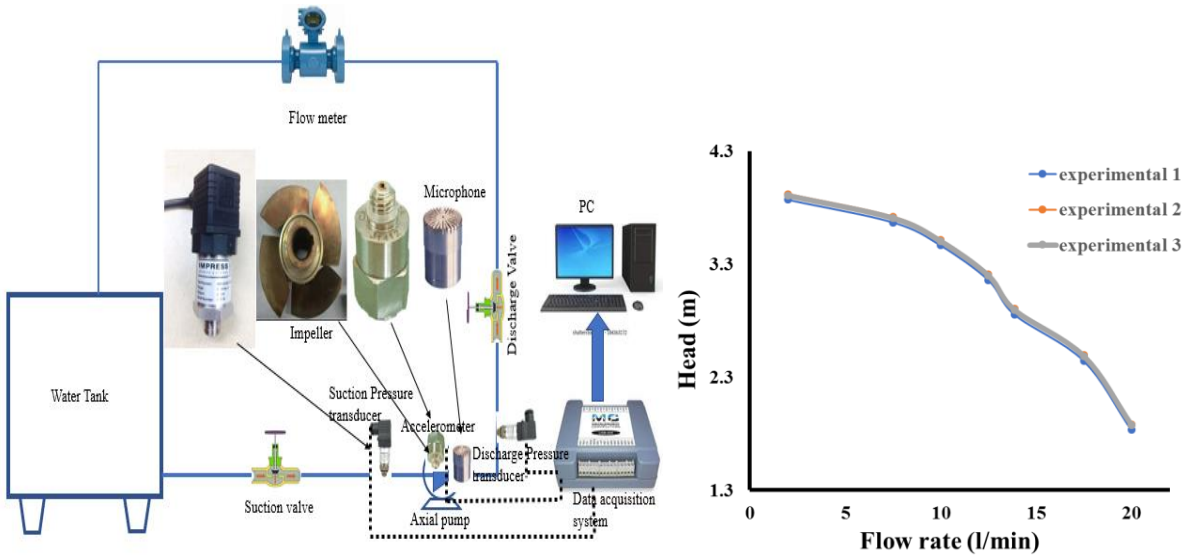

Fig. 3 Diagram of test work loop system and instrumentation and test for the axial flow pump device's repeatability

Fig. 4 Accelerometer, microphone sensors and preamplifier

Table 2 Accelerometer Sensor Specifications

Axial Sensor Sensitivity	100mV/g
Measurement Sensor Range	50g
Transverse Sensitivity	≤5 %
Frequency Response Range (0.5dB)	0.5 to 15,000 Hz
Polarity	Positive
Operating Temperature Range	-40 to +120 °C
Shock Limit (±peak)	3,000g
Operating Accelerometer Current	+2 to +10 mA (typical 4mA)
Output Accelerometer Signal	≤6V
Noise (1 to 20kHz)	＜0.5 mg
Base Strain Accelerometer Sensitivity	0.2mg/με
Magnetic Sensitivity	1.5g/T
Thermal Transient of Sensor Sensitivity	10mg/°C
Output Accelerometer Impedance	＜100 Ω
Weight	9g

sensitivity of the microphone was quantified at 42.00 dBFS. Throughout this research, the ambient temperature was consistently monitored and recorded at 20°C, while the water temperature remained constant at 11°C. The voltage of the pump motor varied for each phase, ranging from 231 V to 235 V. The pump's rotational speed was consistently maintained at 2700 rpm, aligning with the electric motor speed at an AC current frequency of 50 Hz. Tables 2, 3, and 4 show the specifications of the accelerometer, microphone, and pump.

2.2. Methodology of The Data Collection

The experiment began with the pump operating at its optimal efficiency point, as established by the manufacturer's performance curves. This initial phase was designed to collect reference state data and allow sufficient time for the water temperature within the pump body to

Table 3Microphone specifications sensor

Diameter of Microphone	12.7mm (0.50") without grid ;13.2mm (0.52") with grid
Height of Microphone	16.0mm (0.63") without grid; 17.2mm (0.68") with grid;
Microphone Weight	9g
Mounting to amplifier	11.7 mm – 60UNS
Sensing element	Electret condenser
Sensitivity	(250Hz) 31.6mV/Pa (at 250Hz, open-circuit, –30dB±2dB ref.1 V/Pa)
Range of frequency	20Hz to 20kHz
Dynamic range	>140dB SPL within 3% distortion
Thermal noise	<20.0dB
Temperature coefficient 0.01dB within the range	-10ºC and +50ºC

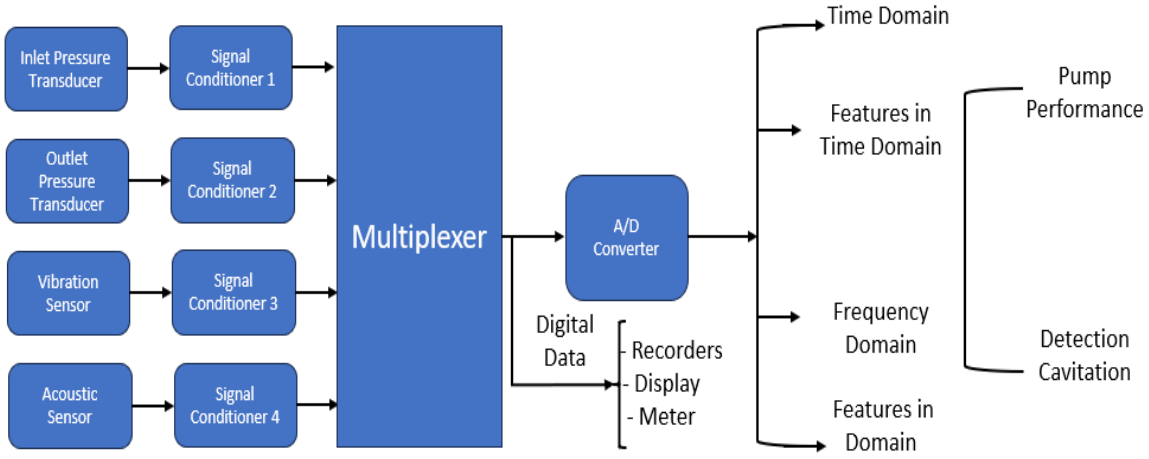

Fig. 5 Analyzing various data in the acquisition system

Table 4 The parts of axial pump with specifications

Part	Value	Unit
Blade angles	60	(degree)
Blades number	Four	(-)
Tip to hub ratio	0.495	(-)
Tip diameter	102	(mm)
Motor power	2.2	(kW)
Hub diameter	50	(mm)
Design speed	3000	(rpm)
Design flow rate	12.5	(l/min)

equalize. Critical performance parameters for the axial pump include total head and efficiency. The calculation of these parameters involves utilizing formulas based on the axial pump's characteristics. Measuring the inlet and outlet pressure is integral to obtaining the head, which essentially involves pressure measurement. To ensure accurate measurements, Impress Control's pressure sensor was employed in accordance with head measurement requirements and relevant standards.

Data can be gathered and recorded using analog devices like a chart recorder for physical signal plotting on paper or display through an oscilloscope. Alternatively, data storage can be achieved through a microprocessor or computer, known as computer data acquisition. This method offers several advantages, including more compact data storage and increased accuracy. It also allows for real-time data processing, enabling efficient utilization of control systems.

A data acquisition system is composed of signal-conditioning units, sensors, and an analog-to-digital converter. As illustrated in Fig. 5, the diagram demonstrates the data acquisition method employed in this project, integrating diverse sensors such as vibration, pressure transducers, and acoustic sensors. The analysis encompasses both frequency

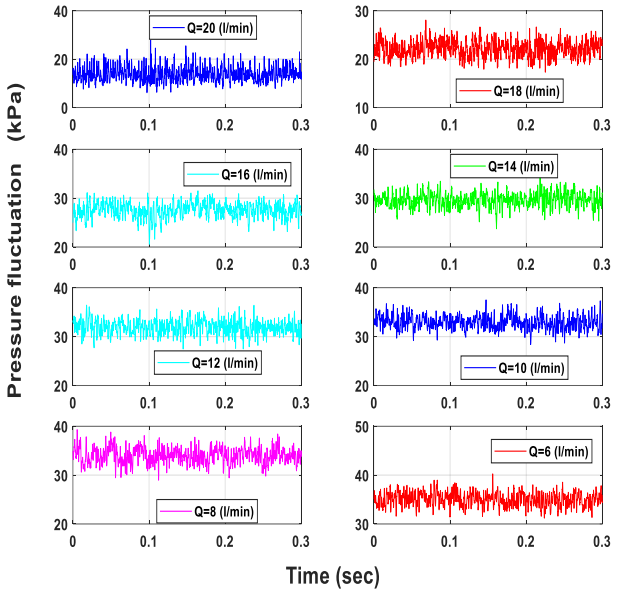

Fig. 6 Variation in pressure fluctuation

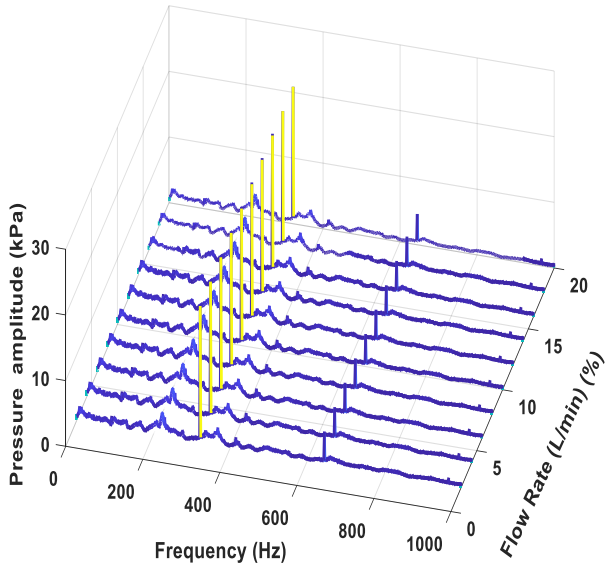

Fig. 7 Frequency domain analysis of pressure signals

and time domains, aiming to compute and forecast pump performance while identifying cavitation in the axial pump.

3. RESULTS OF THE EXPERIMENTAL

This section details the procedure applied to the acceleration and acoustic signals during the tests. The unit was tested under both healthy and cavitation conditions, aiming to extract relevant parameters for pump diagnostics. All presented experimental results were obtained across various operating points for the pump. The transient state duration was set based on different impeller revolutions. Flow was periodic for impeller revolutions, as determined by statistical results and pressure fluctuations across different domains. Subsequently, additional impeller revolutions were computed to conduct a transient statistical analysis on the flow field, encompassing maximum, minimum, and standard deviation features at each condition. To assess the impact of pressure under different conditions in the pump, a comparison of unsteady pressure fluctuations was conducted (refer to Fig. 6) using the experimental flow loop of the axial pump at predefined flow conditions. The results indicate a clear influence of flow conditions (Q representing the flow rate) on pressure fluctuation, where variations in flow conditions correlate with changes in pressure difference. Generally, pressure fields become more intricate as flow rates decrease, especially in the tip region. As flow rates decrease, the pressure difference within a particular flow passage increases, correlating with the pressure fluctuation amplitudes depicted in Fig. 6. During load conditions, vortices are noticeable in the passage. At the design condition, flow instability is not prominent, but a sustained low-pressure area continuously forms.

Frequency domain analysis was employed to depict pressure fluctuations under various conditions, as illustrated in Figure 7. Observations reveal alterations in pressure fluctuations corresponding to distinct flow conditions. Notably, near the tip, the pressure field highlights the existence of a low-pressure area. The variations in pressure amplitudes are attributed to vortex filaments shed from the trailing edge, propagating backward in the flow passage and influencing the shape of the pressure fluctuation curve. As the flow rate decreases relative to Qopt, discernible transient characteristics in pressure fluctuation emerge, primarily influenced by the dissipation and inception of tip cavitation. Concurrently, the gradual increase in the disparity between peaks and troughs becomes apparent. Following a fast Fourier transform, the frequency domains exhibit a consistent trend, with the blade passing frequency standing out as the dominant frequency. Particularly noteworthy is the prevalence of high-frequency components in the frequency domain, especially evident at partial load conditions. This observation signifies a more intricate flow field in the tip region. Furthermore, the amplitudes of dominant frequencies exhibit a decline with increasing flow rates, indicating a correlation with pressure differences that show an increasing trend with decreasing flow rates, aligning well with the temporal revolutions.

In the analysis of pressure fluctuations, experimental results obtained under corresponding conditions were utilized to examine the development of flow fields. Additionally, cavitation data acquired at high speeds and flow rates with synchronized phases were used to support the simulation. The presence of cavitation in the tip region under various conditions is attributed to its association with the curl of the shear layer cavitation, leakage vortex, and clearance cavitation during the rotation of a blade through the acquisition area.

Estimation Technique Based on Q-η and Q-H Curves

Within the monitoring and analysis system for axial pumps, the flow rate is a critical physical parameter. The turbine flowmeter was selected as the flow sensor for this measurement system due to its advantageous characteristics: good repeatability, high accuracy, simple structure, minimal moving parts, high-pressure resistance, wide measuring range, compact size, lightweight design, negligible pressure loss, and ease of maintenance.

In the framework of this experimental investigation, the total head of the axial pump can be computed across different operational scenarios. The suction side velocity is derived using the following equation (Pouffary et al., 2008):

$$V_1 = \frac{4Q}{\pi {d_1}^2} \tag{3}$$

The velocity of this type can be calculated using Equation (4):

$$V_2 = \frac{4Q}{\pi {d_2}^2} \tag{4}$$

Where d_2 and V_2 denote the discharge pipe diameter and the water velocity in the discharge pip, respectively.

Friction Head (Hf)

$$Hf = f\left(\frac{L}{d}\right)\left(\frac{V^2}{2g}\right) \tag{5}$$

Where L, f and d are defined as the pipe length (m), Darcy friction factor, and pipe diameter (m), respectively.

Static Head (Hs)

To determine the total head on the suction pump side, you can employ the following eq. (Pouffary et al., 2008):

$$H_{tin} = Z_1 + \frac{P_1}{\rho g} + \frac{{V_1}^2}{2g} \tag{6}$$

Discharge Side Head

$$H_{tout} = Z_2 + \frac{P_2}{\rho g} + \frac{{V_2}^2}{2g} \tag{7}$$

The pump total head can be computed by following formula (Pouffary et al., 2008).

$$H_t = H_{tin} - H_{tout} - Hf - Hs \tag{8}$$

Where H_{tout} and H_{tin} denote the outlet and inlet head.

In this investigation, the axial pump's cavitation conditions are described by the cavitation coefficient, or σ. The cavitation coefficient σ can be calculated using the following formula (Pouffary et al., 2008):

$$\sigma = \frac{P_{atm} - P_v}{0.5\rho u^2} \tag{9}$$

When both the revolution speed and torque of the axial pump are gauged, the shaft power can be calculated using a designated formula. Hence, measuring the shaft power essentially entails obtaining readings for both the revolution speed and the torque. By adhering to the measurement prerequisites for revolution speed and shaft power, and referring to pertinent standards and regulations, this method facilitates estimating the pump operating point's location. Leveraging the pump curves, alongside the computed head and efficiency pump, the estimated pump speed value is derived.

Since the pump head reflects the total pressure change throughout the pump, as illustrated in Fig. 8, it can be assessed by employing either a pressure differential sensor or two separate pressure sensors situated at the pump's discharge and suction ends (referred to as pressures pd and ps, respectively). This evaluation becomes feasible with an understanding of fluid characteristics, velocity head, and flow losses between the sensors and respective pump flanges. In the context of modern frequency converters, an estimate of the pump speed (n) is conveniently obtainable without requiring additional measurements.

Figure 9 displays the cavitation characteristics observed in this study. It shows the correlation between the required at various head, and cavitation coefficient, providing insight into pump's susceptibility to cavitation.

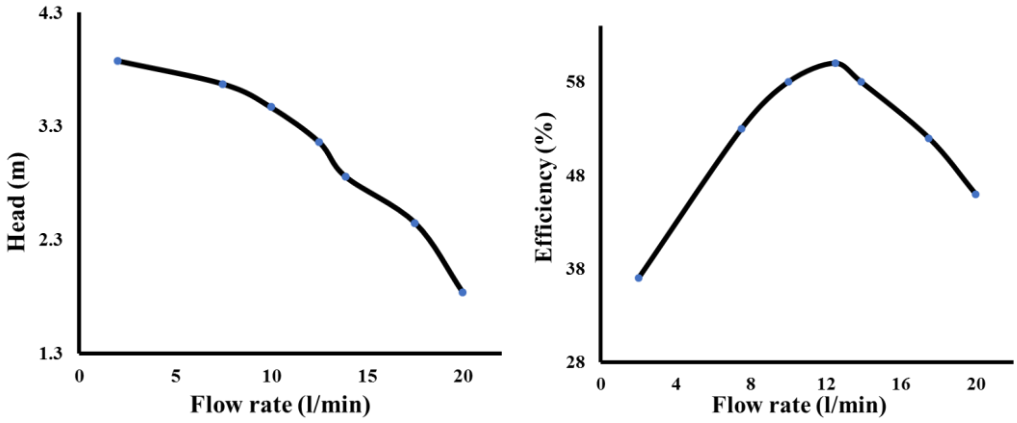

Fig. 8 Performance curves head and efficiency under various pump operating conditions

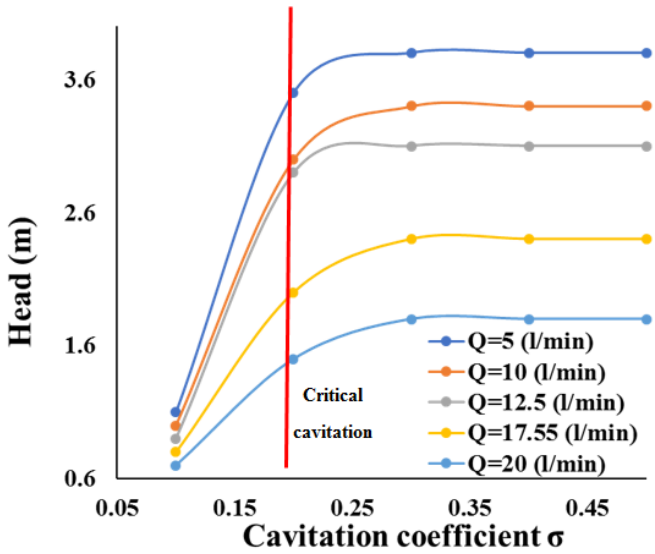

Fig. 9 Cavitation detection with varying flow

Both cavitation coefficient and head were determined through modeling pump system using provided equations. The specifications, types, and cross-sections of all piping systems were defined, and friction losses at each component were calculated. head and cavitation coefficient were computed across different rates of the flow, and the results were graphed against the corresponding flow rates, providing insights obtained from the system modeling, as depicted in this figure.

As shown in the figure, when the flow rate falls below 14 l/min, head exceeds cavitation coefficient. In this scenario, the tested pump operates without encountering cavitation. However, when the flow rate exceeds 16 l/min, the head surpasses cavitation coefficient, indicating cavitation during the pump's operation.

As seen in Fig. 9, the head is essentially steady at first, increases slightly, and then lowers quickly as the cavitation coefficient drops. The primary cause of the stable phenomenon is the low number of cavitation bubbles in the impeller domain during the early stages of cavitation, which has little bearing on the pump device's performance.
A hydraulic smooth zone forms close to the blade surface as the cavitation develops, attaching a mass of cavitation bubbles to the blade surface. This decreases the flow resistance loss near the wall and somewhat raises the head.

3.1. Simulation Signal Vibration and Acoustic Processing

To ensure uniform data collection and maintain a stable water temperature within the pump enclosure, the experiment began by operating the pump at its Best Efficiency Point (BEP), as specified by the manufacturer's performance graphs highlighted in orange in Fig. 10. This figure presents vibration and acoustic data, showing the raw readings under various conditions.

The analysis, as noted from the figure, includes time-domain investigations of both vibration and acoustic signals. To validate the effectiveness of vibration-acoustic denoising methods, a simulated signal with varying flow conditions and a sampling frequency of 40 kHz was utilized. Multiple signals were collected, and Fig. 10 displays two pairs of raw and denoised signals. For each tested condition, the raw signal was decomposed into different components: the periodic part and the residual noise and vibration. The periodic part was extracted by considering different revolutions, while the residual part was determined by subtracting the periodic component from the raw signal.

Figure 11 illustrates the vibration and acoustic data, showcasing these features under varying conditions. The figure displays the characteristics of peak, RMS, peak-to-peak, and variation features for the same data. The amplitude of the vibration and acoustic data varies with changes in flow rate, providing valuable insights into the underlying reasons for these variations. Examining the relationship between the feature values of vibration and acoustic data signals and the pump flow rate offers insights into potential reasons for changes in pump vibration and acoustic data. The figure reveals minimal changes in vibration and acoustic data levels at conditions below 12 l/min. However, at conditions exceeding 14 l/min, there is a substantial rise in vibration and acoustic data levels. A comparison of flow rate values emphasizes a rapid increase in vibration and acoustic levels at higher flow rates. Based on this observation, it can be inferred that analyzing vibration and acoustic data through varying features is a reliable technique for recognizing the onset of cavitation in pumps.

While time-domain trends such as peak, peak-to-peak, RMS, and variations enable the identification of pump cavitation onset, implementing this in practice poses challenges. The limitations inherent in practical pump

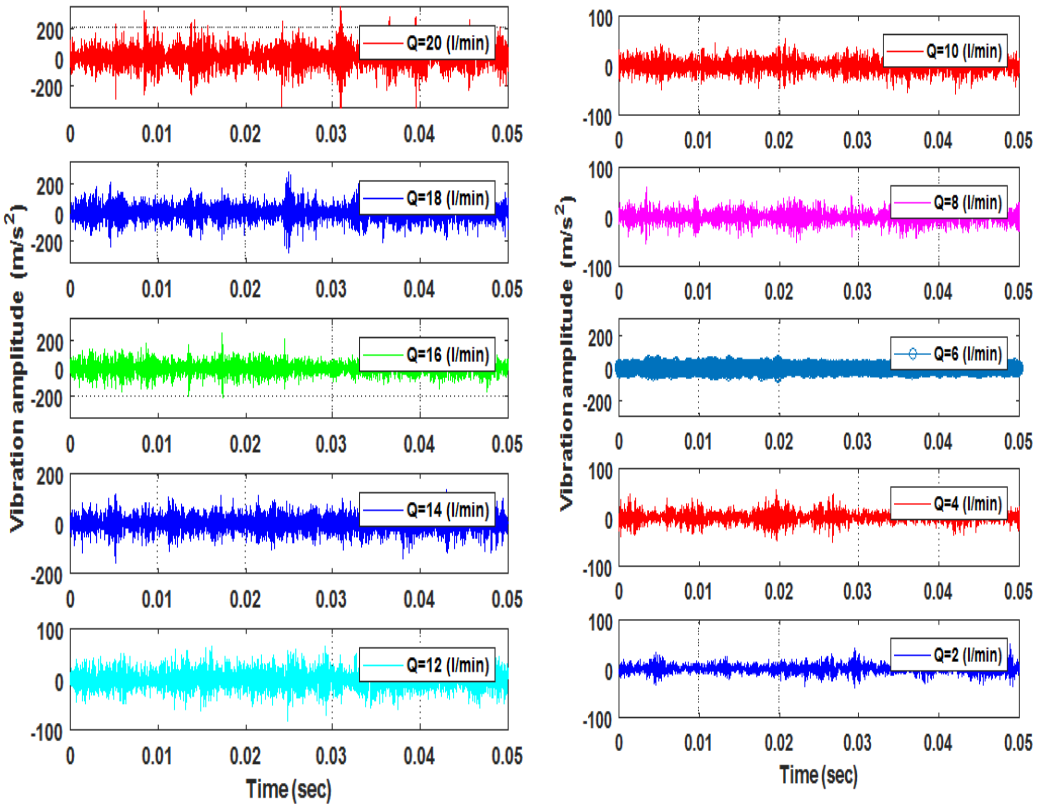

Vibration signals

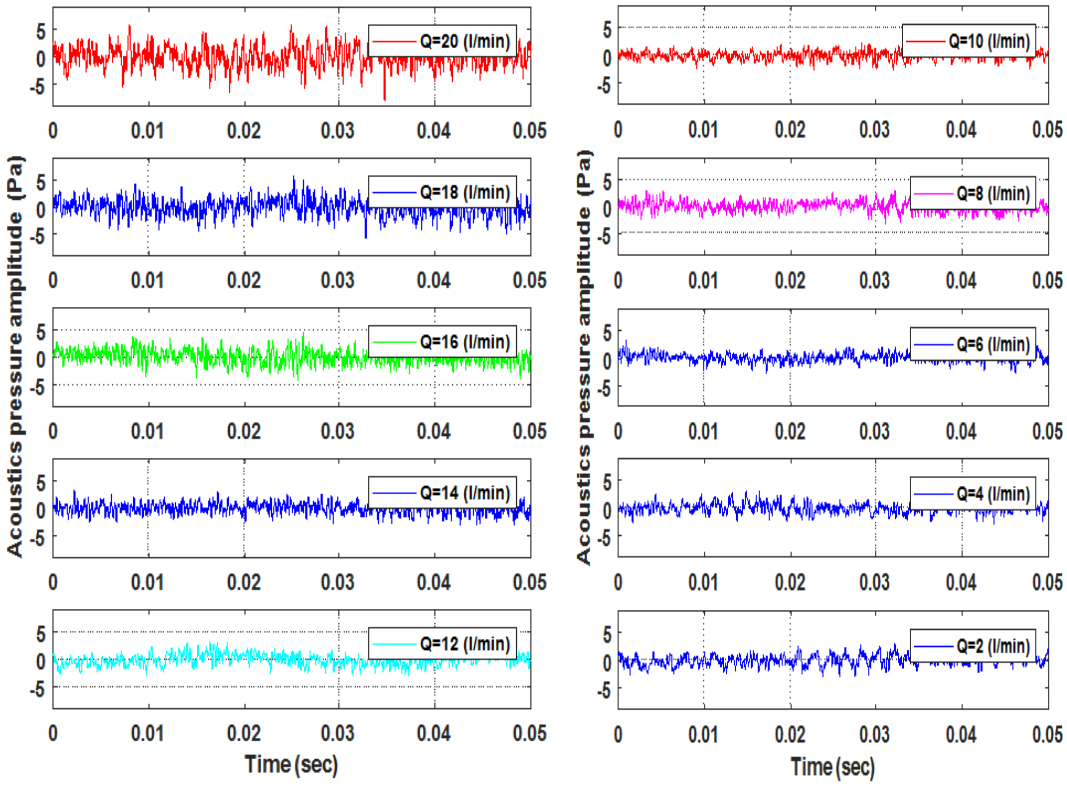

Acoustic signals

Fig. 10 Time-domain plots of vibration and acoustic data

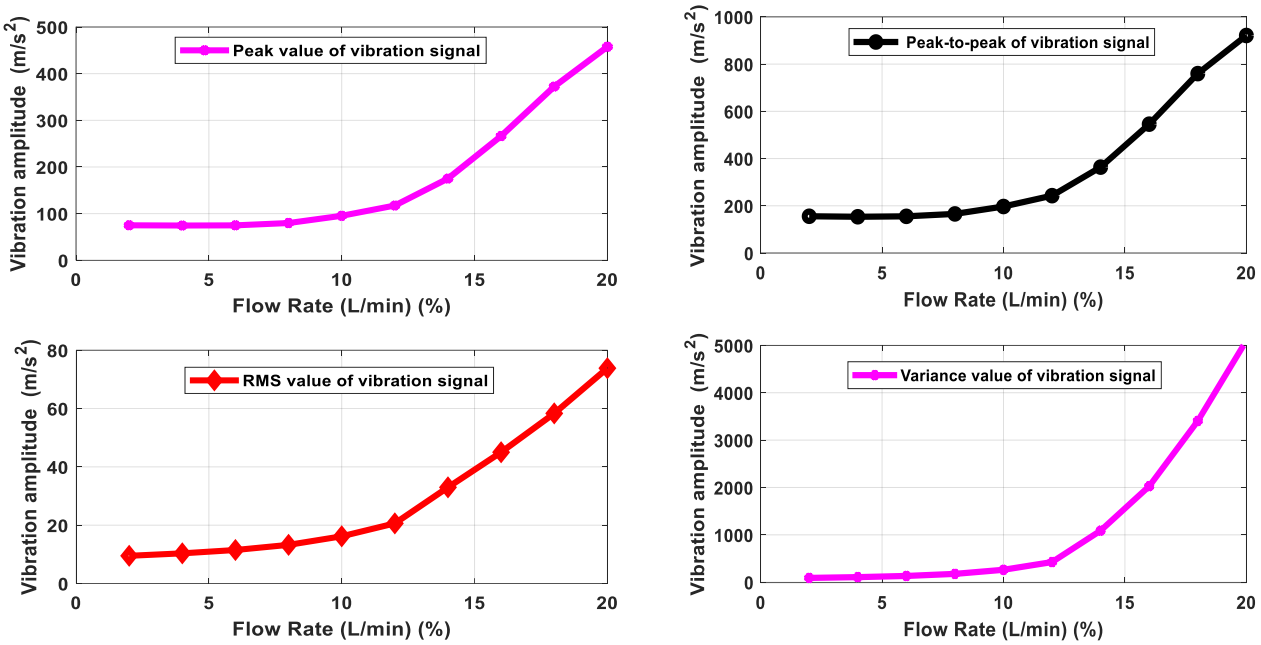

Varying Features in Vibration Signals

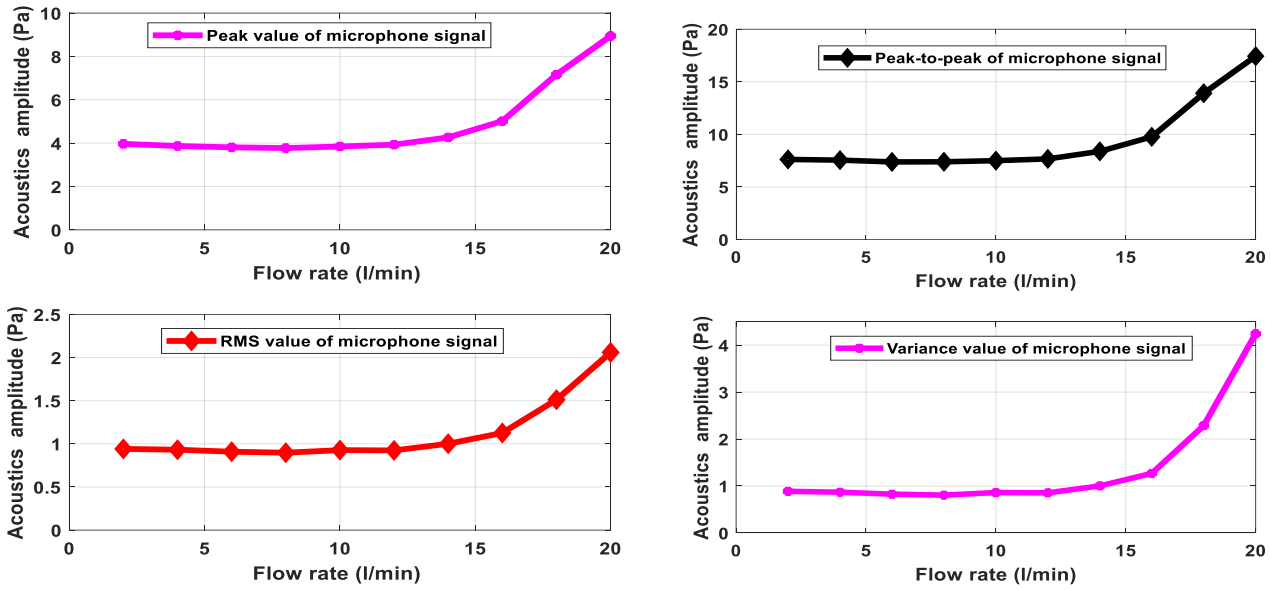

Fig. 11 Trends of features for acoustics and vibration

systems make it difficult to measure data at various flow rates. To improve the prediction and diagnosis of cavitation in axial pumps, clearer features are needed. These features can be uncovered through signal analysis, particularly frequency analysis, focusing on acoustic and vibration signals.

Evaluating data through the root mean square (RMS) value in

$$RMS = \sqrt{\frac{1}{N}\sum_{i=1}^{N} {x_i}^2} \tag{10}$$

The element signal is denoted by x_i, and N represents the total elements.

Analyzing data through the peak-to-peak value and examining data using variance v

$$Variance = \frac{\sum(xi-\bar{x})^2}{N-1} \tag{11}$$

Where xi represents the set of elements, N is total elements, and $\bar{x}$ is mean value of elements.

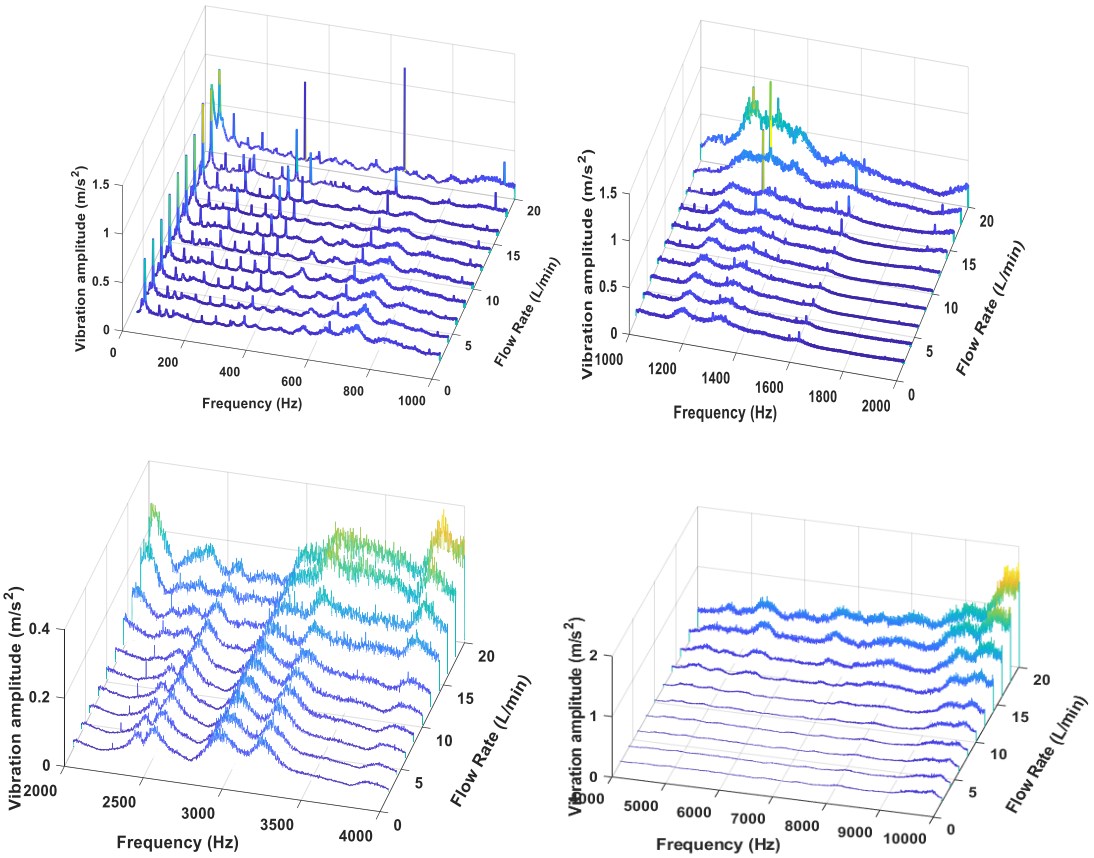

Vibration amplitude across a range of 0 to 10 kHz

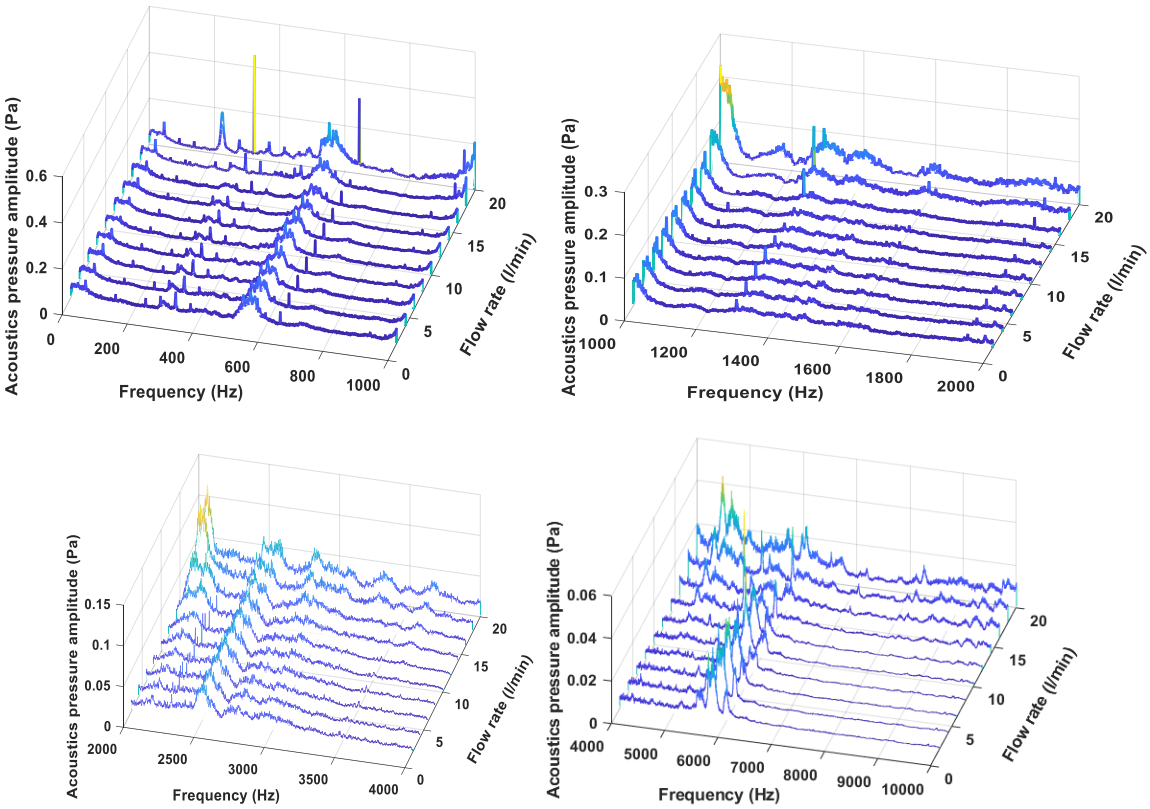

Acoustics amplitude across 0 to 10 kHz

Fig. 12 Amplitude of vibration and acoustics across 0 to 10 kHz range of frequencies

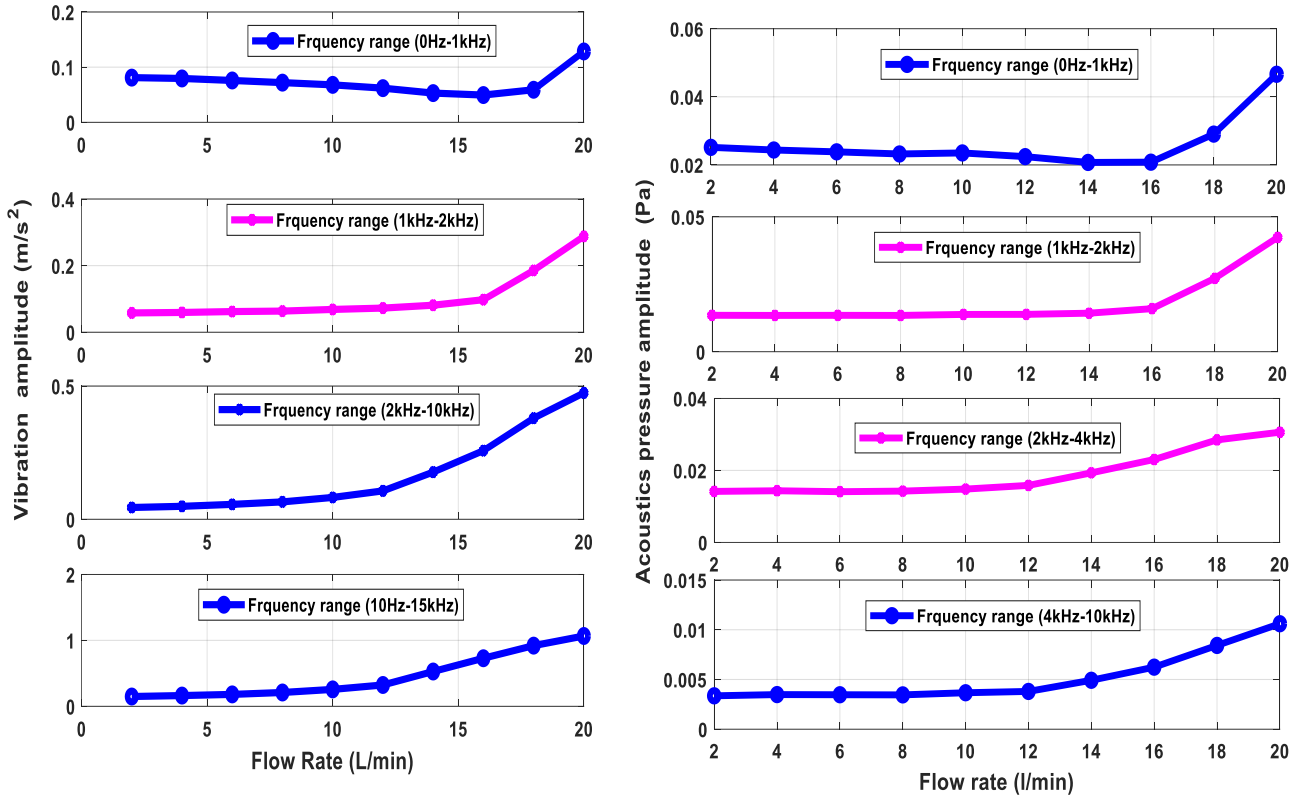

Average amplitude values of vibration

Average amplitude values in acoustics

Fig. 13: Illustration of average vibration and acoustic amplitude values across a diverse frequency range spanning from 0 to 10 kHz

Figure 12 presents the acoustic signals and vibration spectrum at identified flow rates. To compare vibration spectra at different flow rates, a 3D waterfall plot was utilized. This plot facilitates the comparison of multiple spectra, aiding in the identification of amplitude frequencies that remain constant during pump operation (resonance frequency). Figure 12 illustrates the waterfall plots representing the low and high-frequency components of the vibration and acoustic spectrum, respectively.

The figures indicate that at flow rates below 12 l/min, pump vibration and acoustic levels remain relatively constant. However, at flow rates exceeding 14 l/min, there is a notable increase in vibration and acoustic levels, particularly at broadband frequencies above 1 kHz. This rise in pump vibration and acoustic levels corresponds with the cavitation characteristics depicted in the figures.

In this study, a novel approach for detecting cavitation in axial pumps has been developed using vibration and acoustic methods. This approach involves correlating vibration and acoustic amplitudes with pump flow rates, allowing for the synchronization of both acoustic and vibration levels with the cavitation characteristics of the pump. The mean values of the vibration spectrum were utilized for this task.

The mathematical definitions for the Fourier transform and its inverse can be expressed as follows:

$$F(\omega) = \int_{-\infty}^{\infty} X(t) e^{j2\pi * f\, t} dt \tag{12}$$

The inverse of the Fast Fourier Transform (FFT) can be expressed as:

$$X(t) = \int_{-\infty}^{\infty} F(\omega) e^{j2\pi * f\, t} d\omega \tag{13}$$

where, F(ω) and X(t) are the time and frequency signals, and

$$j = \sqrt{-1}$$

In this research, frequency ranges below 10 kHz were utilized in conjunction with broadband analysis. This approach helps minimize the cost of the required sensors and reduces computational efforts. The figure depicts the acoustic spectrum amplitudes and mean values of vibration with flow rate, showcasing the low-frequency amplitude (0 to 1 kHz) and the high-frequency amplitude (4 to 10 kHz). Figure 13 highlights that the minimum levels of acoustic frequency and vibration occur at a flow rate of 12 l/min.

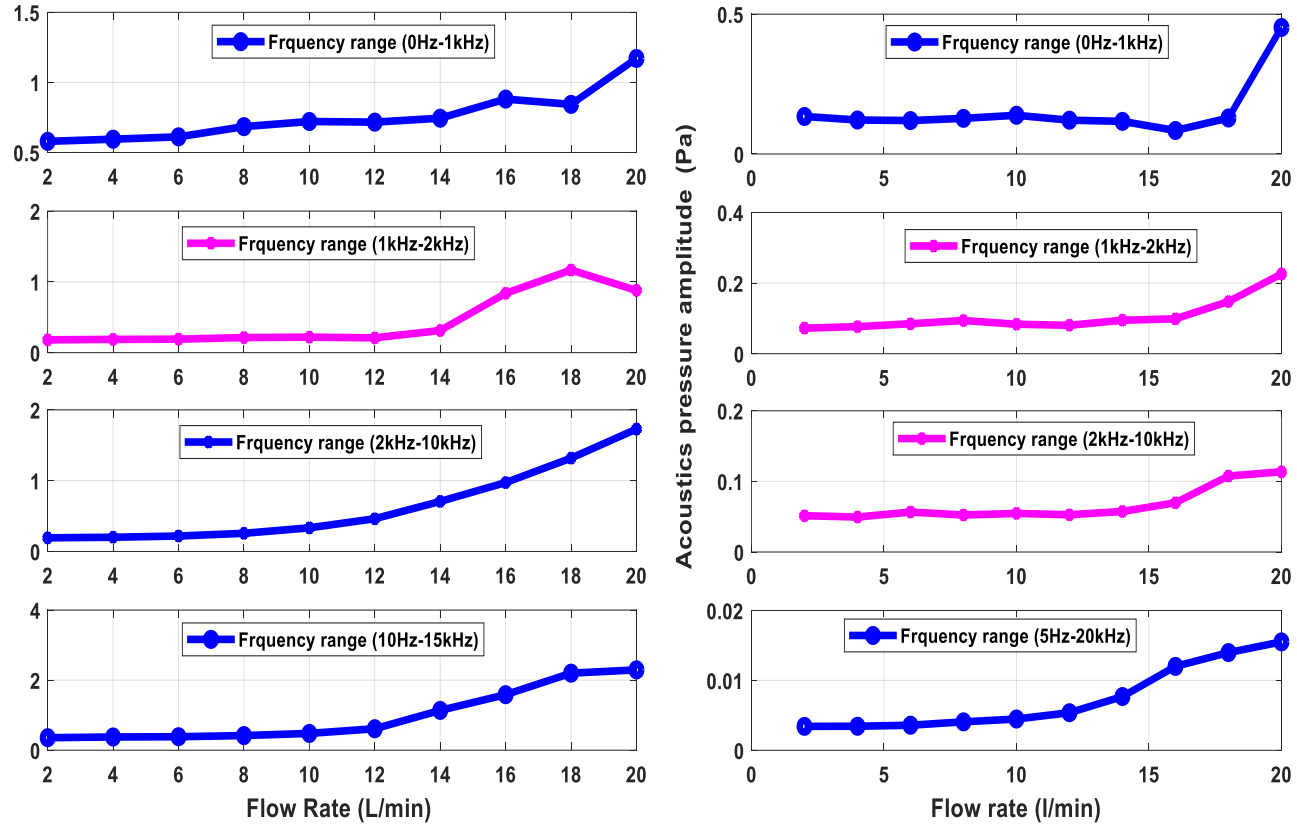

Peak amplitude values of vibration

Peak amplitude values in acoustics

Fig. 14 Maximum vibration and acoustic amplitude values across a diverse frequency range from 0 to 10 kHz

This outcome aligns with the analyses presented in the preceding figures. The vibration and acoustic data at both high and low-frequency ranges exhibit a sudden increase when the flow rate exceeds 16 l/min. This study reveals that vibration and acoustic amplitudes can serve as thresholds for detecting the onset of cavitation, with amplitudes surpassing this threshold indicating the severity of cavitation. Moreover, the vibration and acoustic data analysis suggests that this conclusion is not limited to a specific frequency range but can be achieved using various frequency ranges, including 0-4 kHz. Figure 14 illustrates the graphs of the mean values of vibration and acoustic amplitudes over the frequency ranges of 1-2 kHz and 4-10 kHz, respectively. These findings suggest that all frequency ranges produce results comparable to the broadband frequency range. Consequently, vibration and acoustic sensors operating at lower frequency ranges can effectively detect cavitation in an axial pump, potentially reducing the overall expenses associated with high-frequency sensors.

The analysis of peak amplitude values in the vibration and acoustic spectrum across various frequency ranges (0-10 kHz) demonstrates that the observed outcome is applicable across the entire frequency spectrum, not limited to a specific range. Figure 14 illustrates the relationship between peak amplitude values of vibration and noise levels within the frequency ranges of 0-1 kHz, 1-2 kHz, 2-4 kHz, and 4-10 kHz. These figures highlight that all frequencies in an axial pump can be effectively detected using relatively affordable vibration and acoustic sensors. The correlation between flow rate and signals at different frequency ranges (0-10 kHz) shown in this figure indicates a consistent increase in pump vibration and acoustics at flow rates exceeding 14 l/min. In summary, the findings suggest that utilizing mean and peak features in frequency domain analysis enables early detection of cavitation in pumps across various frequency ranges, particularly in the low-frequency range, allowing for the use of cost-effective vibration and acoustic sensors.

4. CONCLUSIONS

This experimental investigation yields several key findings pertinent to the aims of this research:

1. The flow rate of 16 l/min emerged as a critical reference point for all analyses, signifying the onset of cavitation. The tested pump operates without encountering cavitation; however, when the flow rate exceeds 16 l/min, the NPSHR surpasses the NPSHA, indicating cavitation during the pump's operation.

2. Cavitation detection in axial pumps through the analysis of acoustics and vibration signals yields similar results. Primary indicators, such as peak, peak-to-peak, RMS, and variations values, serve as effective metrics for cavitation detection. Broadband frequencies (2 kHz – 10 kHz) and the low-frequency range (0 – 1 kHz) in frequency-based analysis reveal clear trends related to cavitation presence. The distinguishing factor between vibration and acoustics methods lies in the former's greater effectiveness in predicting pump performance and detecting cavitation. This advantage positions vibration as the preferred method, especially in scenarios where access to the monitored machine is challenging.

3. Analysis of vibration signals in the time domain proves effective in detecting and diagnosing cavitation in axial pumps. Employing mean and peak values for vibration and acoustics amplitude analysis in the frequency domain provides additional insights for predicting cavitation.

4. The vibration and acoustics data at both high and low frequency ranges exhibit a sudden increase when the flow rate exceeds 16 l/min, due to the occurrence of cavitation. The severity of cavitation can be inferred by observing increased levels of vibration and acoustics amplitude values, offering a reliable indication of cavitation severity on the pump.

5. The analysis of variations in vibration and acoustics amplitudes under different experimental flow rates aligns with cavitation characteristics predicted by pressure signals, NPSHa, and NPSHr.

ACKNOWLEDGMENTS

In this recent research work, the authors wish to more acknowledge the Mustansiriyah University Baghdad – Iraq (www.uomustansiriyah.edu.iq) for their support.

CONFLICT OF INTEREST

The authors in this work declared that there is no conflict of interest.

AUTHOR CONTRIBUTION STATEMENT

The all authors confirm contribution to the paper as follows: study conception and design, data collection, analysis and interpretation of results, draft manuscript preparation. All authors reviewed the results and approved the final version of the manuscript.

REFERENCES

Adeodu, A., Daniyan, I., Omitola, O., Ejimuda, C., Agbor, E., & Akinola, O. (2020). An adaptive Industrial Internet of things (IIOts) based technology for prediction and control of cavitation in axialpumps. *Procedia CIRP*, *91*, 927-934. http://creativecommons.org/licenses/by-nc-nd/4.0/

Coutier-Delgosha, O., Fortes-Patella, R., Reboud, J. L., Hakimi, N., & Hirsch, C. (2005). Stability of preconditioned Navier–Stokes equations associated with a cavitation model. *Computers & Fluids*, *34*(3), 319-349. https://doi.org/10.1016/j.compfluid.2004.05.007

Hallaji, S. M., Fang, Y., & Winfrey, B. K. (2022). Predictive maintenance of pumps in civil infrastructure: State-of-the-art, challenges and future directions. *Automation in Construction*, *134*, 104049. https://doi.org/10.1016/j.autcon.2021.104049

Harihara, P. P., & Parlos, A. G. (2008, January). *Sensorless detection of impeller cracks in motor driven axialpumps.* ASME International Mechanical Engineering Congress and Exposition (Vol. 48661, pp. 17-23). https://doi.org/10.1115/IMECE2008-66273

Katz, J. (1984). Cavitation phenomena within regions of flow separation. *Journal of Fluid Mechanics*, *140*, 397-436. https://doi.org/10.1017/S0022112084000665

Kunz, R. F., Boger, D. A., Stinebring, D. R., Chyczewski, T. S., Lindau, J. W., Gibeling, H. J., ... & Govindan, T. (2000). A preconditioned Navier–Stokes method for two-phase flows with application to cavitation prediction. *Computers & Fluids*, *29*(8), 849-875. https://doi.org/10.1016/S0045-7930(99)00039-0

Laberteaux, K. R., Ceccio, S. L., Mastrocola, V. J., & Lowrance, J. L. (1998). High speed digital imaging of cavitating vortices. *Experiments in Fluids*, *24*(5-6), 489-498. https://doi.org/10.1007/s003480050198

Mousmoulis, G., Karlsen-Davies, N., Aggidis, G., Anagnostopoulos, I., & Papantonis, D. (2019). Experimental analysis of cavitation in a axialpump using acoustic emission, vibration measurements and flow visualization. *European Journal of Mechanics-B/Fluids*, *75*, 300-311. https://doi.org/10.1016/j.euromechflu.2018.10.015

Oza, M. N., & Shah, D. S. (2020, November). *Theoretical and experimental modal analysis of axialpump radial flow impeller*. IOP Conference Series: Materials Science and Engineering (Vol. 992, No. 1, p. 012003). IOP Publishing. https://doi.org/10.1088/1757-899X/992/1/012003

Pouffary, B., Patella, R. F., Reboud, J. L., & Lambert, P. A. (2008). Numerical simulation of 3D cavitating flows: analysis of cavitation head drops in turbomachinery.

Schnerr, G. H., & Sauer, J. (2001, May). *Physical and numerical modeling of unsteady cavitation dynamics.* Fourth international conference on multiphase flow (Vol. 1). New Orleans, LO, USA: ICMF New Orleans.

Sendilvelan, S., & Prabhahar, M. (2017). Pre-stress modal analysis of a axialpump impeller for different blade thicknesses. *International Journal of Mechanical and Production Engineering Research and Development*, *7*, 507-516. https://doi.org/10.24247/ijmperddec201758

Shagluf, A., Parkinson, S., Longstaff, A. P., & Fletcher, S. (2018). Adaptive decision support for suggesting a machine tool maintenance strategy: from reactive to preventative. *Journal of Quality in Maintenance Engineering*, *24*(3), 376-399. https://doi.org/10.1108/JQME-02-2017-0008

Tian, Y., & Hu, A. (2018). Study on critical speed of rotation in the multistage high speed axialpumps rotors. *International Journal of Heat & Technology*, *36*(1), 31-39. https://doi.org/10.18280/ijht.360105

Xu, C., Zhou, H., & Mao, Y. (2020). Analysis of vibration and noise induced by unsteady flow inside a axialcompressor. *Aerospace Science and Technology*, *107*, 106286. https://doi.org/10.1016/j.ast.2020.106286

Zhang, Y., Liu, J., Yang, X., Li, H., Chen, S., Lv, W., ... & Wang, D. (2022). Vibration analysis of a high-pressure multistage axialpump. *Scientific Reports*, *12*(1), 20293. http://creativecommons.org/licenses/by/4.0/